Electronic Supplementary Material (ESI) for ChemComm.

Supporting information

Continuous catalytic upgrading of ethanol to n-butanol over Cu-CeO_2/AC catalysts

Dahao Jiang, Xianyuan Wu, Jun Mao, Jun Ni*, Xiaonian Li*

State Key Laboratory Breeding Base of Green Chemistry Synthesis Technology, Institute of Industrial Catalysis, Zhejiang University of Technology, Hangzhou 310014, China

E-mail addresses: junni@zjut.edu.cn (J. Ni), xnli@zjut.edu.cn (X. Li).

Table of Contents

1. Experimental methods

Catalyst preparation. Cu-CeO_2/AC catalysts with 10 wt.% of Cu loading and different molar ratios of Cu/Ce were prepared by a wetness impregnation method as follows: AC supports were impregnated with appropriate amount of ethanol solution of $Cu(NO_3)_2 \cdot 3H_2O$ and $Ce(NO_3)_3 \cdot 6H_2O$ for 4 h. Excess solvents were then removed at 298 K in a rotary evaporator. The resultant composite was dried in ambient air at 383 K for 4 h and subsequently calcined in nitrogen flow at 723 K for 2 h in a tube furnace**.** Cu-CeO_2/SiO_2 and Cu-CeO_2/Al_2O_3 with Cu/Ce molar ratio of 3:1, as well as Cu/AC and Cu/CeO_2 with Cu loading of 10 wt.%, were prepared by the same method as reference. These catalysts with the different molar ratios of Cu/Ce are designated as xCuyCe/z; here x:y indicates the molar ratio of Cu/Ce, while z indicates AC, SiO_2 and Al_2O_3.

Catalyst characterization. The parameters of pore structure of catalysts were determined by N_2 adsorption using Quantachrome NOVA 1000e apparatus with liquid-N_2 at the temperature of 77 K. The samples were outgassed at 473 K for 4 h prior to analysis. XRD data were collected on an X'Pert PRO X-ray diffractometer between $2\theta = 10^o$ and 80^o at 2^o min^{-1} employing a Cu-Kα radiation source (λ = 0.15406 nm). Transmission electron microscopy (TEM) observation and corresponding elemental analysis were performed on an instrument (Tecnai G2 F30 S-Twin, 300 kV) from Philips-FEI Company.

TPR and CO_2-TPD experiments were performed on a TPR/TPD apparatus made in our lab. Hundred milligrams of the samples were placed in a quartz reactor and reduced by a 10% H_2-Ar gas mixture in a flow rate of 30 ml/min with temperature ramping at 10 K/min. By using a thermal conductivity detector (TCD) to monitor the outlet gases after cold traps (to remove H_2O), TPR profiles were obtained. For CO_2-TPD experiments, catalysts were pre-reduced for 1 h in a flow of 10% H_2-Ar gas mixture at 523 K, purged by Ar at the same temperature for 0.5 h, and then cooled

down to 323 K. The CO_2 saturation uptake of the reduced catalysts was achieved by passing pure CO_2 for 0.5 h at 30 ml/min. After the CO_2 adsorption, the catalyst was purged again by He for 30 min at 323 K. Then the temperature was linearly increased from 323 K to 1073 K at 10 K/min, while CO_2-TPD profiles were recorded with the TCD.

Catalytic test. The catalytic tests were performed in a fixed-bed reactor. Typically, 1.0g of catalyst (20-40 mesh) was placed in a tubular reactor (30 cm length, 8 mm internal diameter) and then was reduced by a 10% H_2-N_2 gas mixture at 523 K for 1 h. The reaction was carried out under the following conditions: 523 K, 2 MPa, LHSV=4 ml/(h·g cat) and N_2/ethanol = 500:1 (v/v). The liquid products were analyzed by a Gas chromatograph (GC) with a flame ionization detector (FID) and an HP-5 column (30 m, 0.25 mm inner diameter) or an FFAP column (30 m, 0.25 mm inner diameter). 2-ethyl-hexanol was used as the internal standard for the quantification of the liquid products. The outlet gases from the condenser were analyzed by the GC with a TCD and an HP-PLOT/Q column (30 m, 0.32 mm inner diameter).

The ethanol conversion, selectivity and yield of products are calculated as follows：

$$\text{Ethanol conversion (\%)} = \frac{1 - C\ mol\ of\ unreacted\ ethanol}{C\ mol\ of\ (products + unreacted\ ethanol)} \times 100\%$$

$$\text{Product selectivity (\%)} = \frac{C\ mol\ of\ \text{specific}\ product}{C\ mol\ of\ products} \times 100\%$$

$$\text{Product yield (\%)} = \text{Ethanol conversion} \times \text{Product selectivity}$$

where C mol is the mole number of carbon in the products and unreacted ethanol.

Kinetic experiments. Kinetic measurements for various reaction components (ethanol dehydrogenation/ acetaldehyde condensation/ crotonaldehyde hydrogenation) were separately carried out using the same fixed-bed reactor described above. Kinetic data were obtained with different contact times and feedstock partial pressures by

varying the flow rates of carrier gases and feedstock. For example, the overall aldehyde yields with different contact times and different ethanol partial pressures were gained by varying the flow rates of N_2 and ethanol. Specifically, for acetaldehyde condensation, toluene and 10 vol.% acetaldehyde in toluene were independently introduced into a N_2 stream flowing at given flow rates using two syringe pumps, while cyclohexane and 10 vol.% crotonaldehyde in cyclohexane were individually introduced into a H_2 stream flowing for crotonaldehyde hydrogenation. For the studies of reaction kinetics, the system was allowed to reach steady-state under constant reaction conditions before recording the kinetic data. The analytic methods of products were the same as those stated in the catalytic test.

For the analysis of kinetic data, function-curves for the overall yields of the dehydrogenation, condensation or hydrogenation products to W/F were first gained by data fitting. And then reaction rates of above three reactions were calculated by taking the derivative of functions of the overall yields to W/F.

The rate constants and reaction orders at different temperatures for various reactions were achieved by fitting the data groups of both logarithm of reaction rates and partial pressures of feedstock. Finally, the apparent activation energies and frequency factors for various reaction components were achieved by drawing the Arrhenius plots.

2. Ethanol conversion and n-butanol yield over Cu-CeO_2/AC catalysts with the different Cu/Ce molar ratios

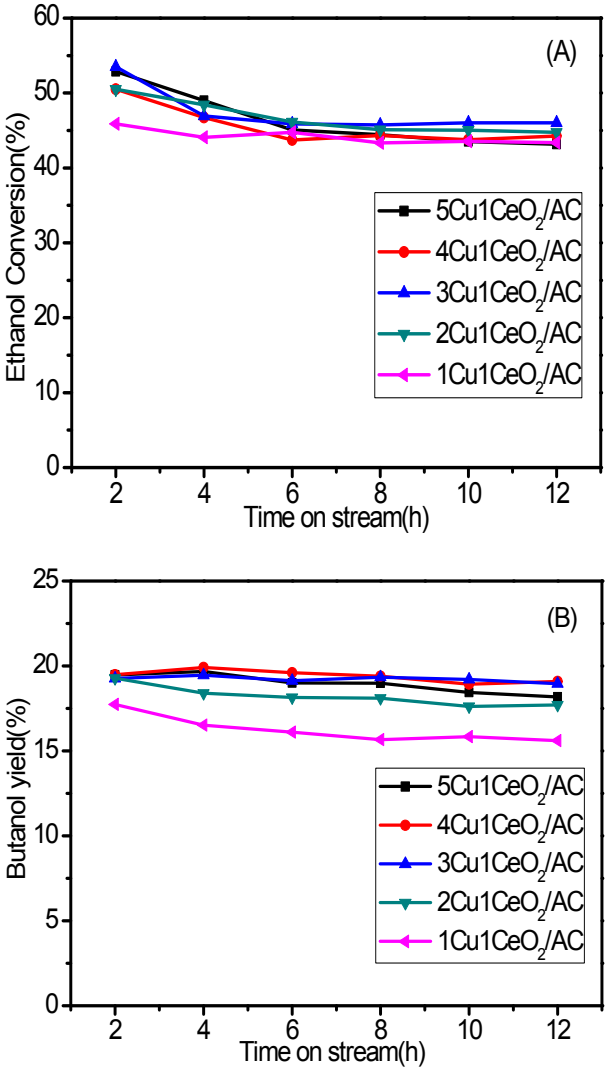

Fig. S1. Ethanol conversion (A) and n-butanol yield (B) over Cu-CeO_2/AC catalysts with the different Cu/Ce molar ratios

3. XRD patterns of reduced catalysts before and after reaction

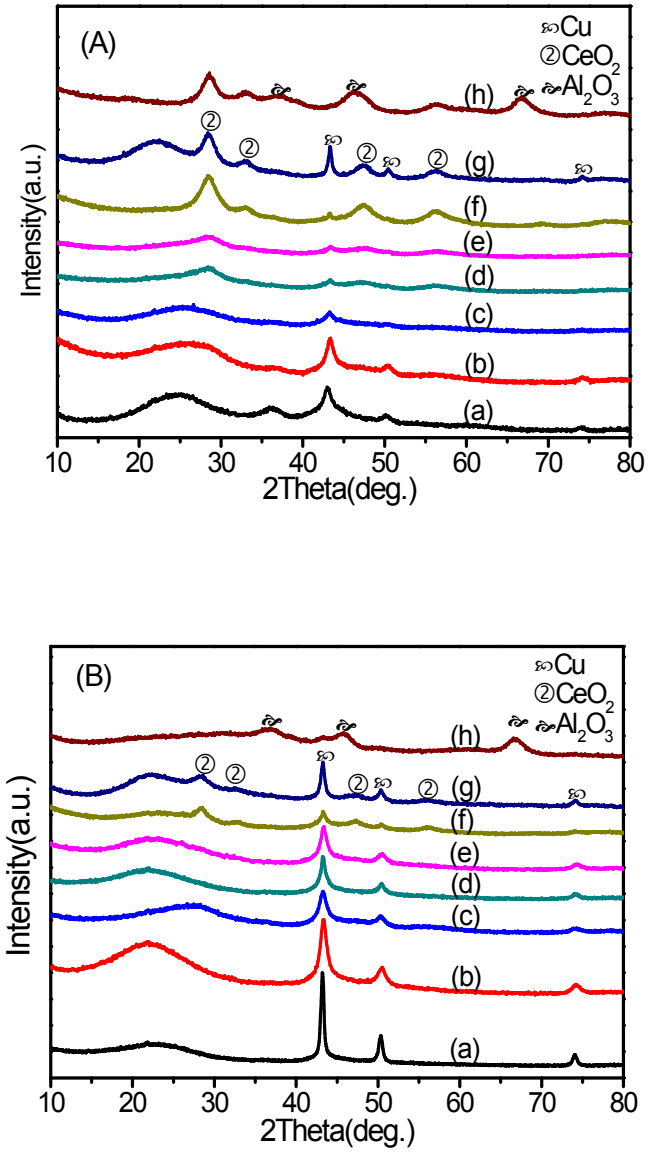

Fig. S2. XRD patterns of reduced catalysts (A) before and (B) after reaction: (a)Cu/AC; (b)5Cu1Ce/AC; (c)4Cu1Ce/AC; (d)3Cu1Ce/AC; (e)2Cu1Ce/AC; (f)1Cu1Ce/AC; (g)3Cu1Ce/SiO_2; (h)3Cu1Ce/Al_2O_3

4. CO_2-TPD profile of AC support

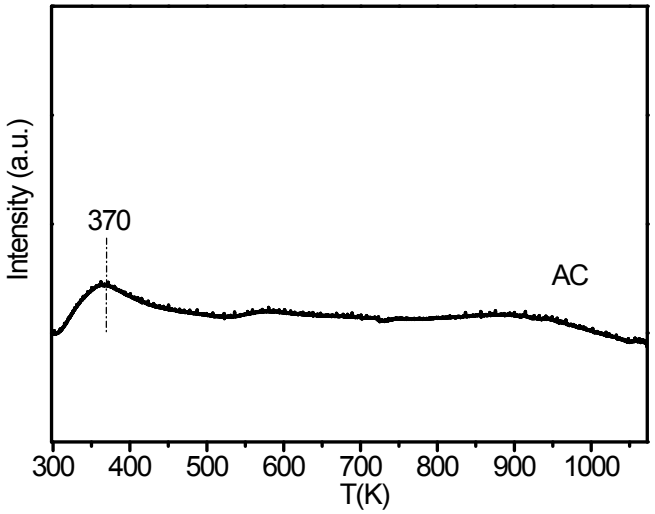

Fig. S3. CO_2-TPD profile of AC support

5. CO_2-TPD profile of CeO_2/AC

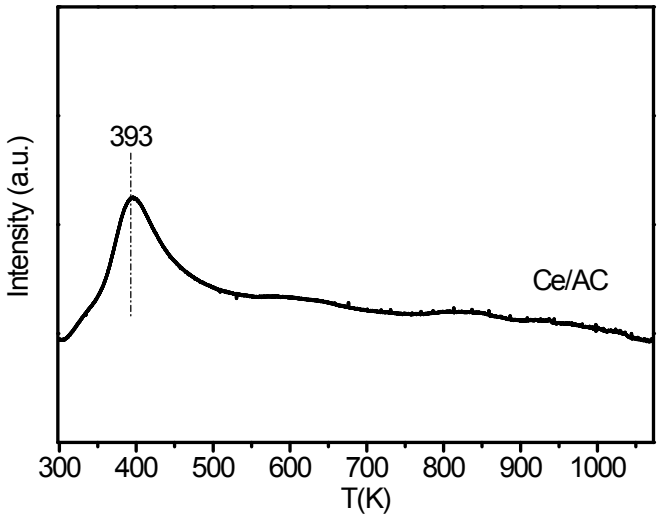

Fig. S4. CO_2-TPD profile of CeO_2/AC

6. TPR profile of AC support

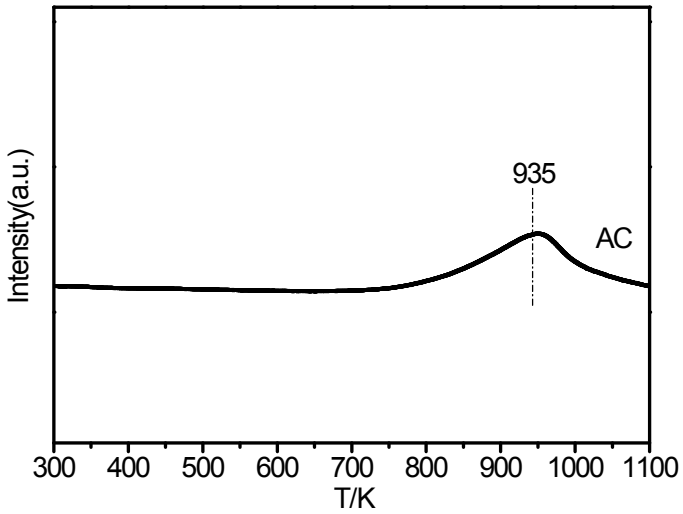

Fig. S5. TPR profile of AC support

7. TPR profile of CeO_2/AC

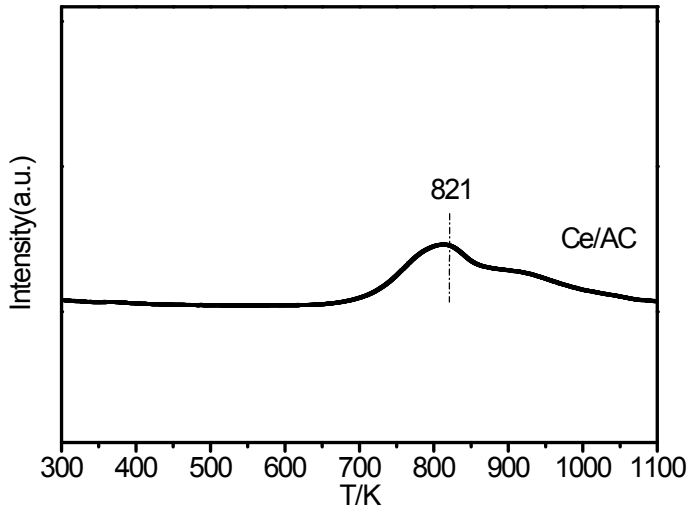

Fig. S6. TPR profile of CeO_2/AC

8. TEM images and corresponding EDX mapping of (A), (B) 3Cu1Ce/SiO_2 and (C), (D) 3Cu1Ce/Al_2O_3 catalysts after reaction

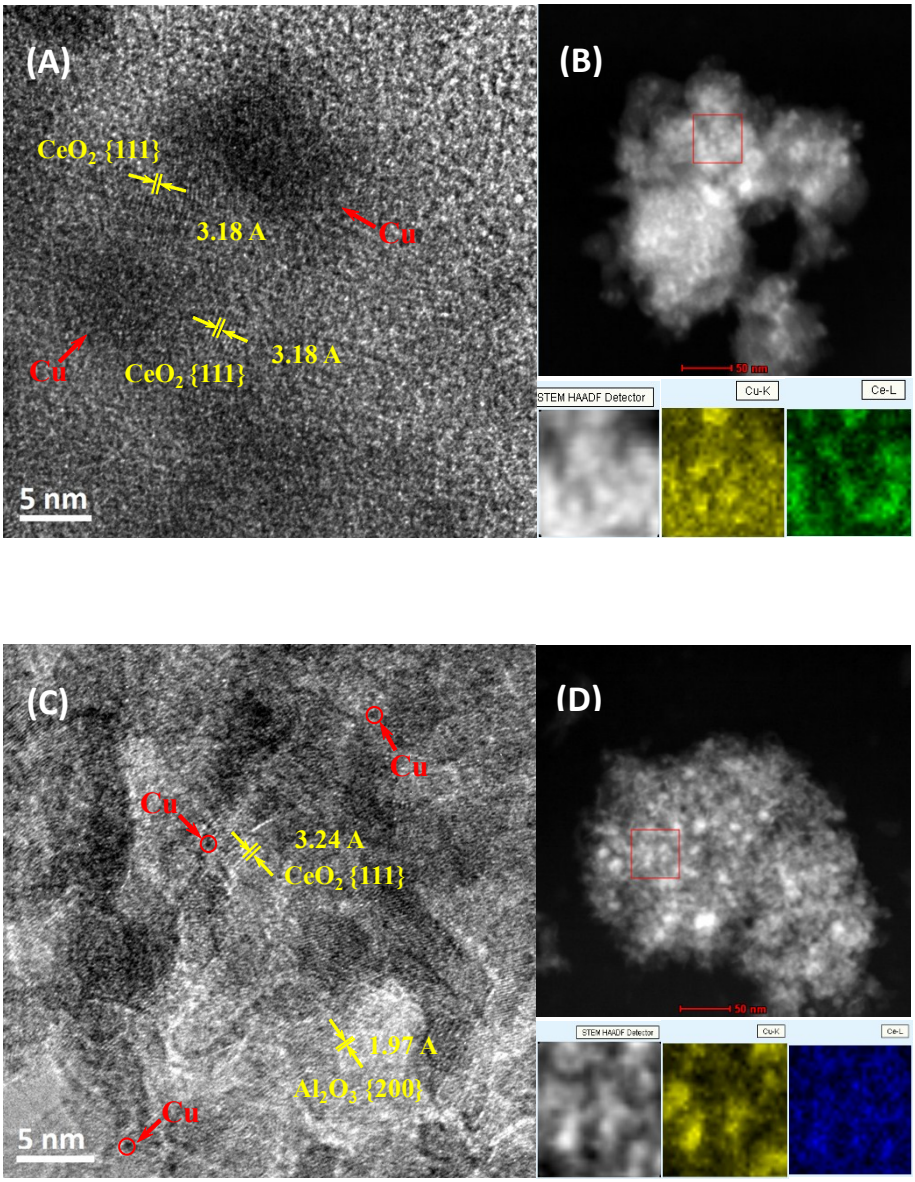

Fig. S7. TEM images and corresponding EDX mapping of (A), (B) 3Cu1Ce/SiO_2 and (C), (D) 3Cu1Ce/Al_2O_3 catalysts after reaction

For the 3Cu1Ce/SiO_2 catalyst, the average particle size of Cu metals was calculated around 15 nm (Fig. S7A), which is larger than that of Cu (9.1 nm) on 3Cu1Ce/AC catalyst with the same Cu loading and Cu/Ce molar ratio. There also exists some

crystal CeO_2 with size of 4.0 nm in the vicinity of the Cu metal particles, which is also larger than that of CeO_2 (1.8 nm) on 3Cu1Ce/AC catalyst. It should be noted that no structure in which Cu metals are partially covered by crystal CeO_2 is present in Figure S7A. Moreover, no significant expansion of the interplannar spacing of CeO_2 {111} can be observed, suggesting the absence of incorporation of Cu in the crystal lattice of CeO_2. This can be also evidenced by comparing the basicity of catalysts in CO_2-TPD that a lower CO_2 desorption temperature is observed on 3Cu1Ce/SiO_2 relative to 3Cu1Ce/AC catalyst. The corresponding EDX mapping further illustrates that the distribution of CeO_2 is uneven and does not match that of Cu metals (Fig. S7B), indicating that the contact of Cu with CeO_2 is less than the case of 3Cu1Ce/AC catalyst. These results emphasize the importance of the close contact between Cu with CeO_2 that the strong interaction of Cu with CeO_2 can not only suppress the sintering of Cu and growth of CeO_2, but also increase the basicity of CeO_2.

For the 3Cu1Ce/Al_2O_3 catalyst, small Cu metals with size of less than 1 nm can be observed (Fig. S7C). These small Cu metals are uniformly spread over the catalyst even after the reaction. Only trace of crystal CeO_2 can be spotted near Cu metals on this catalyst. Since clear characteristic diffraction peaks assignable to CeO_2 (corresponding to 3.8 nm) can be observed on the reduced catalyst before reaction (Fig. S2), the existence of tiny amounts of crystal CeO_2 is likely due to the phase transition from crystalline to amorphous during the reaction. Nevertheless, the expansion of the interplannar spacing of CeO_2 {111} from 3.12 to 3.24 Å implies the strong interaction between Cu metals and CeO_2. The EDX mapping reveals a heterogeneous distribution of CeO_2 over this catalyst and a poor overlap between Cu and CeO_2 signals (Fig. S7D). Comparing the particle size of Cu metals on 3Cu1Ce/Al_2O_3 with 3Cu1Ce/AC catalyst (<1.0 nm vs. 9.1 nm), in which the latter having a strong interaction between Cu and CeO_2, Al_2O_3 has a better capability of stabilizing Cu against sintering than CeO_2. Thus, majority of Cu metals are in contact with Al_2O_3, although some are incorporated in the crystal lattice of CeO_2.

Based on the above analysis, we concluded that Cu metals in contact with Al_2O_3 (in the case of 3Cu1Ce/Al_2O_3) have the better stability than with CeO_2 (in the case of 3Cu1Ce/AC), followed by SiO_2 (in the case of 3Cu1Ce/SiO_2). According to the extent of Cu incorporation in the crystal lattice of CeO_2 and the distribution of Cu and CeO_2, 3Cu1Ce/AC has the highest amount of CeO_2 with strong basicity among the three catalysts, followed by 3Cu1Ce/Al_2O_3 with less amount of strong basic CeO_2, while 3Cu1Ce/SiO_2 has the lowest amount of medium/weak basic CeO_2. This trend is evidenced by CO_2-TPD experiment (Fig. 1A) and also reflected in the variation of the selectivity towards C-C coupling product n-butanol (41.3% on 3Cu1Ce/AC, 12.1% on 3Cu1Ce/Al_2O_3 and 10.2% on 3Cu1Ce/SiO_2).

9. Dependence of the hydrogenation of crotonaldehyde on reaction temperature

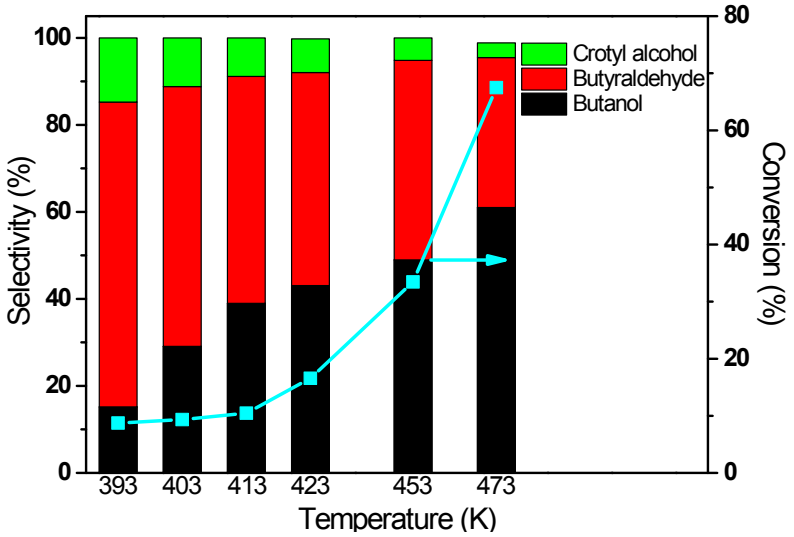

Fig. S8. Dependence of the hydrogenation of crotonaldehyde on reaction temperature: catalyst, 0.1g; 2 MPa; H_2, 30 ml/min; 3.94 vol.% crotonaldehyde in cyclohexane, 0.304 ml/min.

10. Function-curves for the overall yield of aldehyde ($Y_{aldehyde}$) to W/F

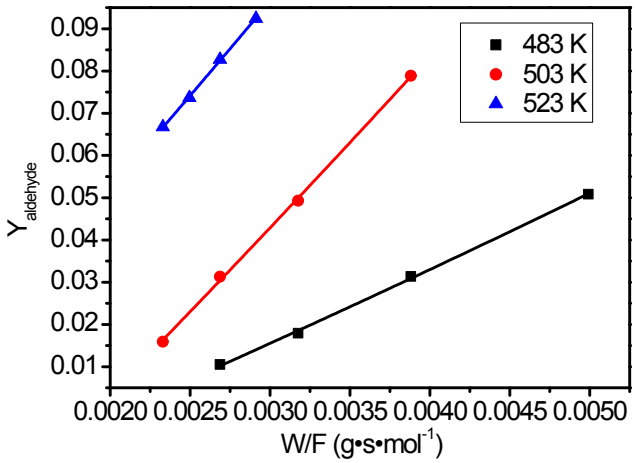

Fig. S9. Function-curves for the overall yield of aldehyde ($Y_{aldehyde}$) to W/F

11. Function-curves for the logarithm of reaction rate of ethanol dehydrogenation ($lnr_{aldehyde}$) to the logarithm of partial pressure of ethanol ($lnP_{ethanol}$)

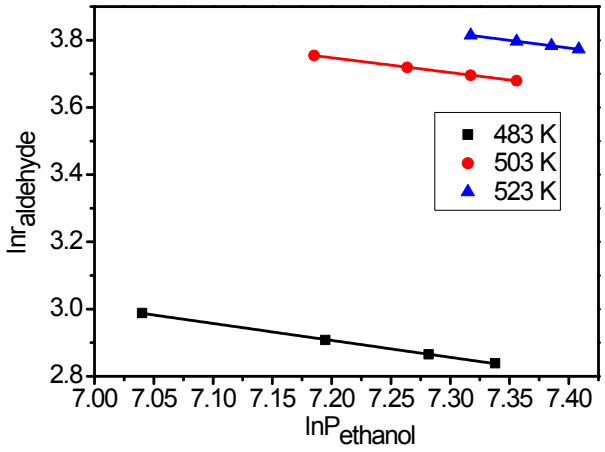

Fig. S10. Function-curves for the logarithm of reaction rate of ethanol dehydrogenation ($lnr_{aldehyde}$) to the logarithm of partial pressure of ethanol (lnPethanol)

12. Function-curves for the overall yield of condensation products ($Y_{condensation}$) to W/F

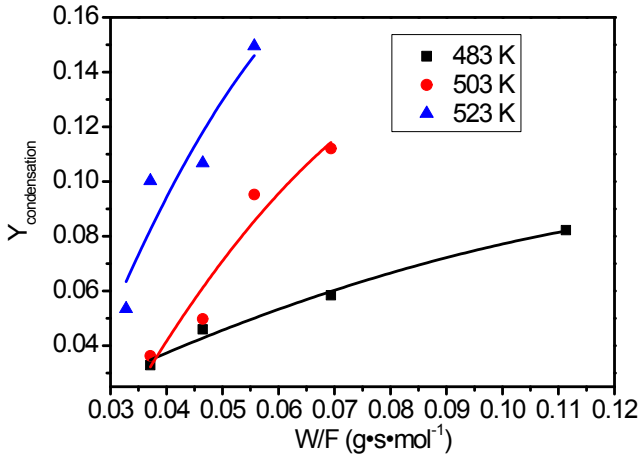

Fig. S11. Function-curves for the overall yield of condensation products ($Y_{condensation}$) to W/F

13. Function-curves for the logarithm of reaction rate of aldehyde condensation ($lnr_{condensation}$) to the logarithm of partial pressure of aldehyde ($lnP_{aldehyde}$)

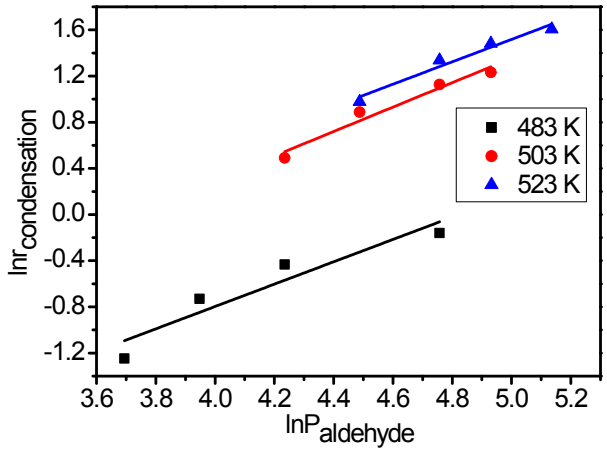

Fig. S12. Function-curves for the logarithm of reaction rate of aldehyde condensation ($lnr_{condensation}$) to the logarithm of partial pressure of aldehyde ($lnP_{aldehyde}$)

14. Function-curves for the overall yield of hydrogenation products ($Y_{hydrogenation}$) to W/F

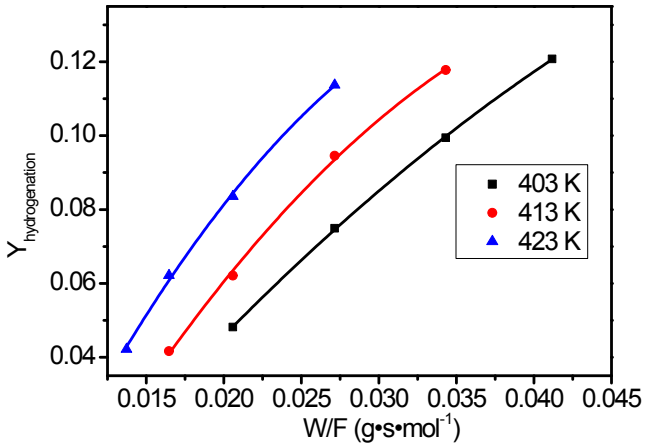

Fig. S13. Function-curves for the overall yield of hydrogenation products ($Y_{hydrogenation}$) to W/F

15. Function-curves for the logarithm of reaction rate of crotonaldehyde hydrogenation ($lnr_{hydrogenation}$) to the logarithm of partial pressure of crotonaldehyde ($lnP_{crotonaldehyde}$)

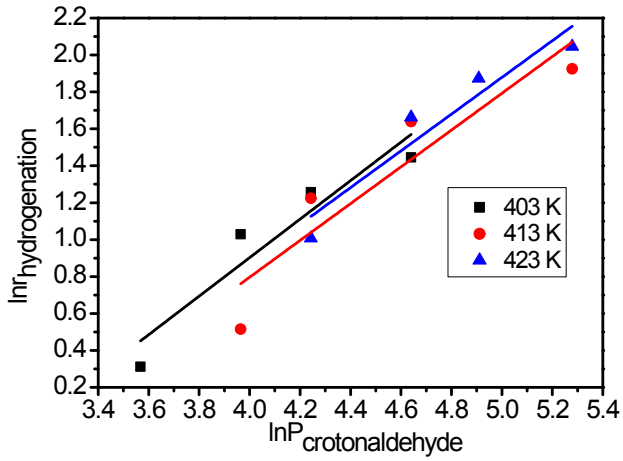

Fig. S14. Function-curves for the logarithm of reaction rate of crotonaldehyde hydrogenation ($lnr_{hydrogenation}$) to the logarithm of partial pressure of crotonaldehyde ($lnP_{crotonaldehyde}$)

16. Arrhenius plots for (A) ethanol dehydrogenation, (B) aldehyde condensation and (C) crotonaldehyde hydrogenation

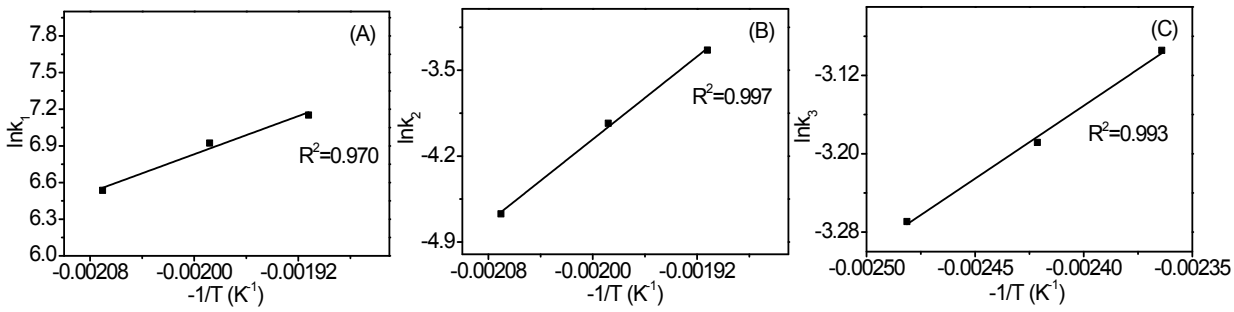

Fig. S15. Arrhenius plots for (A) ethanol dehydrogenation, (B) aldehyde condensation and (C) crotonaldehyde hydrogenation

17. Textural properties of Cu-based catalysts

Table S1. Textural properties of Cu-based catalysts

Catalyst	S_{BET}[a]	V_t[b]	D_{pore}[c]	d_{Cu}[d] (nm)		d_{CeO2}[d] (nm)	
	(m^2g^{-1})	(cm^3g^{-1})	(nm)	XRD	TEM	XRD	TEM
Cu/AC	952.8	0.52	2.7	22(4.3)	22.6	-	-
5Cu1Ce/AC	877.5	0.48	2.7	9.2(5.9)	10.4	-	-
4Cu1Ce/AC	862.9	0.48	2.8	8.7(5.3)	9.0	-	-
3Cu1Ce/AC	861.0	0.47	2.8	8.7(5.1)	9.1	(1.5)	(1.8)
2Cu1Ce/AC	783.8	0.43	2.8	8.6(5.1)	9.1	(1.8)	(2.2)
1Cu1Ce/AC	707.9	0.39	2.9	8.3(4.9)	8.6	4.2(4.5)	4.9(4.8)
3Cu1Ce/SiO_2	277.0	0.82	11.9	15.2(14.6)	16.0	3.9(4.0)	4.0(4.0)
3Cu1Ce/Al_2O_3	190.5	0.50	10.4	-	-	(3.8)	(3.8)

[a] Brunauer-Emmett-Teller surface area. [b] Total pore volume. [c] The average pore diameters. [d]The value in bracket is the average particle diameter of the reduced catalyst before reaction.

18. Catalytic performance of various Cu-based catalysts

Table S2. Catalytic performance of various Cu-based catalysts[a]

Catalyst	Conversion (%)	Selectivity(%)						Butanol Yield (%)
		Acetaldehyde	Butyraldehyde	Ethyl Acetate	Butanol	C6 products[b]	Others[c]	
CeO_2/AC	3.1	13.5	4.4	2.2	1.6	4.9	73.4	-
Cu/AC	1.2	10.5	0.5	0.5	12.1	-	76.4	0.1
Cu/CeO_2	11.7	37.7	8.8	19.9	21.1	2.8	9.9	2.5
3Cu1Ce/AC	46.2	7.2	7.8	10.9	41.3	19.7	13.0	19.1

[a] Conversion, selectivity and yield are obtained at steady-state; reaction conditions: catalyst, 1.0 g; 523 K, 2 MPa (N_2), LHSV=4 ml/(h·g·cat), N_2/ethanol(v/v)=500:1;
[b] C6 products include 2-ethylbutyraldehyde, hexaldehyde, 2-ethylbutanol, and 1-hexanol;
[c] Other products include 1-ethoxyethane, 1,1-diethoxyethane, butyl acetate, etc; specially for CeO_2/AC, 12.3% diethyl ether, 50% crotonaldehyde, 2.1% 1,1-diethoxyethane; for Cu/AC catalyst, 2.6% 1-ethoxyethane, 55.3% 1,1-diethoxyethane; for Cu/CeO_2 catalysts, 6.1% diethyl ether, 1.7% 1,1-diethoxyethane.

In comparison of the catalytic performance of Cu/CeO_2 with Cu/AC, the ethanol conversion is higher on Cu/CeO_2 (11.7%) than Cu/AC (1.2%), which indicates a better dispersion of Cu metals in Cu/CeO_2 than Cu/AC as a result of stronger metal-support interaction. Besides, the selectivity towards butanol is also higher on Cu/CeO_2 (21.1%) than Cu/AC (12.1%), suggesting the higher

basicity of Cu/CeO_2 than Cu/AC. When supporting Cu and CeO_2 on activated carbon, as in the case of 3Cu1Ce/AC, the selectivity towards butanol is almost doubled to 41.3% whereas the selectivity towards acetaldehyde decreases 5 times from 37.7% to 7.2%. The significant enhancement of selectivity towards butanol is likely due to the presence of acidic functional groups in activated carbon which promotes the dehydration reaction in the condensation process (Scheme S1) and drives the reaction equilibrium towards the formation of crotonaldehyde. Additionally, the activated carbon support further improves the dispersion of Cu metals, leading to much higher ethanol conversion and consequent higher butanol yield.

Moreover, comparing Cu/AC with 3Cu1Ce/AC catalyst, it is evident that the addition of Ce also improves 39 times of the ethanol conversion from 1.2 to 46.2%. This significant enhanced dehydrogenation rate of ethanol is also the result of reaction equilibrium shift towards acetaldehyde consumption when the aldol condensation is promoted by the presence of Ce species. Kinetic analysis supports that the aldol condensation is the decisive step in Guerbet reaction pathway for n-butanol production. The introduction of Ce species significantly lowers the apparent activation energy for aldol condensation in comparison to that over hydroxyapatite [ACS Catal. 2016, 6, 939-948]. Therefore, the presence of Ce species not only raises the selectivity towards n-butanol production, but also improves the ethanol conversion, thus the overall n-butanol yield is promoted.

19. Comparison of catalytic performance of Cu-CeO_2/AC catalysts with other catalysts reported in documentary

Table S3. Comparison of catalytic performance of Cu-CeO_2/AC catalysts with other catalysts reported in documentary

Catalyst	T (K)	P (MPa)	Other reaction conditions	Ethanol Conversion (%)	Butanol Selectivity (%)	Butanol Yield (%)	Conversion · liquid hourly space velocity (10^{-2} mol·g^{-1}·h^{-1})	Ref
Rb-Na X zeolite	693	0.1	W/F=5.6 g·h·mol^{-1}	0.21	40.9	0.86	0.04	1
MgO	723	0.1	0.5 g catalyst W/F=20.83 g·h·mol^{-1}	56.14	32.76	18.39	2.69	2
3Mg1AlO	623	0.1	W/F=23.33 g·h·mol^{-1}	33.2	34.3	11.39	1.42	3
HAP (Ca/P=1.64)	573	0.1	Contact time = 1.78 s	14.7	76.3	11.22	Unknown	4
HAP (Sr/P=1.70)	573	0.1	W/F=130 g·h·mol^{-1}	11.3	86.4	9.76	0.09	4
HTC-500 20.7%Ni/Al_2O_3	513	7	W/F=11.11 g·h·mol^{-1}	10	69	6.9	0.90	6
Cu/HSACeO_2	533	10	LHSV=1.97 h^{-1}	67	44.8	30	-	7
Cu-CeO_2/AC	523	2	W/F=14.30 g·h·mol^{-1} (LHSV=2 h^{-1})	45.6	42.4	19.3	3.18	This work
Pd-Mg-Al-O	473	0.1	0.5 g catalyst 39.5 g ethanol Reaction time 5 h	3.8	72.7	2.76	1.31	3
HTC-500 20.7%Ni/Al_2O_3	523	7	3.3 g catalyst 80 g ethanol reaction time = 72 h	25	80	20	0.18	5
Cu-CeO_2/AC	523	0.1	3.3 g catalyst 80 g ethanol reaction time = 12 h	35.1	49.8	17.5	1.54	This work
Cu-CeO_2/AC	523	0.1	3.3 g catalyst 80 g ethanol reaction time = 48 h	39.1	55.2	21.6	0.43	This work

The comparison of catalytic performance in fixed-bed reactors is summarized in the first part of Table S3, while those in batch reactors is compiled in the second part. Our Cu-CeO_2/AC catalyst exhibits the highest reaction rate and butanol yield among all other catalysts in fixed-bed reactions. In batch reactor, we have performed the reaction in 12 h and 48 h separately. After 12 h of reaction, up to 17.5% of butanol yield can be obtained with the highest reaction rate among other catalysts. Further increasing the reaction time to 48 decreases the average reaction rate but raises the butanol yield to the highest 21.6%. The decrease in the average reaction rate is probably due to the more competitive adsorption of ethanol with other reaction

intermediates and products on Cu-CeO_2/AC catalyst after 12 h of reaction. As provided by kinetic analysis, the enhanced reaction rate and butanol yield are fundamentally ascribed to the much lower apparent activation energies for ethanol dehydrogenation, aldol condensation and rehydrogenation.

20. Experiment data for macro-kinetics of ethanol dehydrogenation

Table S4. Experiment data for macro-kinetics of ethanol dehydrogenation[a]

number	T (K)	F_{N2} (ml/min)	$F_{ethanol}$ (ml/min)	$W/F \cdot 10^{-3}$ (g·s/μmol)	$P_{ethanol}$ (kPa)	$Y_{aldehyde}$ (%)
1	483	44.0	0.35	4.9910	1505	5.08
2	483	56.8	0.45	3.8819	1505	3.13
3	483	69.4	0.55	3.1761	1505	1.79
4	483	82.4	0.65	2.6874	1505	1.05
5	483	69.4	0.24	7.2785	1142	9.09
6	483	69.4	0.36	4.8523	1332	7.37
7	483	69.4	0.48	3.6392	1454	4.32
8	483	69.4	0.6	2.9114	1538	3.01
9	503	56.8	0.45	3.8819	1505	7.88
10	503	69.4	0.55	3.1761	1505	4.93
11	503	82.4	0.65	2.6874	1505	3.13
12	503	94.7	0.75	2.3291	1505	1.59
13	503	69.4	0.35	4.9910	1320	11.93
14	503	69.4	0.45	3.8819	1428	8.22
15	503	69.4	0.55	3.1761	1506	4.61
16	503	69.4	0.65	2.6874	1565	2.84
17	523	76.0	0.6	2.9114	1505	9.24
18	523	82.4	0.65	2.6874	1505	8.27
19	523	88.3	0.7	2.4955	1505	7.37
20	523	94.7	0.75	2.3291	1505	6.67
21	523	69.4	0.55	3.1761	1506	13.55
22	523	69.4	0.65	2.6874	1565	7.43
23	523	69.4	0.75	2.3291	1612	5.10
24	523	69.4	0.85	2.0551	1650	4.15

[a] 3Cu1Ce/AC catalyst (80-100 mesh), 0.5 g; 2 MPa; F_{N2}, flow rate of nitrogen; $F_{ethanol}$, flow rate of ethanol; $P_{ethanol}$, partial pressure of ethanol; $Y_{aldehyde}$, overall yield of aldehyde

21. Experiment data for macro-kinetics of acetaldehyde condensation

Table S5. Experiment data for macro-kinetics of acetaldehyde condensation[a]

number	T (K)	F_{N2} (ml/min)	$F_{aldehyde}$ (ml/min)	$W/F \cdot 10^{-2}$ (g·s/μmol)	$P_{aldehyde}$ (kPa)	$Y_{condensation}$ (%)
1	483	34.1	0.008	11.1336	88.9	8.22
2	483	54.6	0.012	6.9357	88.9	5.84
3	483	81.9	0.018	4.6492	88.9	4.59
4	483	102.3	0.023	3.7112	88.9	3.29
5	483	68.2	0.007	12.6292	40.2	4.65
6	483	68.2	0.009	9.7259	51.8	4.73
7	483	68.2	0.012	7.2321	69.1	6.55
8	483	68.2	0.020	4.1889	116.4	6.96
9	503	54.6	0.012	6.9357	88.9	11.20
10	503	68.2	0.015	5.5668	88.9	9.52
11	503	81.9	0.018	4.6492	88.9	4.97
12	503	102.3	0.023	3.7112	88.9	3.62
13	503	68.2	0.012	7.2321	69.1	5.05
14	503	68.2	0.015	5.5668	88.9	8.21
15	503	68.2	0.020	4.1889	116.4	9.16
16	503	68.2	0.024	3.4821	138.4	6.81
17	523	68.2	0.015	5.5668	88.9	14.95
18	523	81.9	0.018	4.6492	88.9	10.67
19	523	102.3	0.023	3.7112	88.9	10.03
20	523	116.0	0.026	3.2797	88.9	5.35
21	523	68.2	0.015	5.5668	88.9	12.41
22	523	68.2	0.020	4.1889	116.4	13.84
23	523	68.2	0.024	3.4821	138.4	17.99
24	523	68.2	0.030	2.7834	170.0	19.62

[a] 3Cu1Ce/AC catalyst (80-100 mesh), 0.25 g; 2 MPa; F_{N2}, flow rate of nitrogen; $F_{aldehyde}$, flow rate of aldehyde; $P_{aldehyde}$, partial pressure of aldehyde; $Y_{condensation}$, overall yield of condensation products including crotonaldehyde, butyraldehyde, crotonyl alcohol and butanol.

22. Experiment data for macro-kinetics of crotonaldehyde hydrogenation

Table S6. Experiment data for macro-kinetics of crotonaldehyde hydrogenation[a]

number	T (K)	F_{H2} (ml/min)	$F_{crotonaldehyde}$ (ml/min)	$W/F \cdot 10^{-2}$ (g·s/μmol)	$P_{crotonaldehyde}$ (kPa)	$Y_{hydrogenation}$ (%)
1	403	30.0	0.012	4.1176	69.5	12.08
2	403	36.0	0.014	3.4314	69.5	9.94
3	403	45.0	0.018	2.7149	69.5	7.49
4	403	60.0	0.024	2.0588	69.5	4.81
5	403	60.0	0.008	6.1765	35.4	11.33
6	403	60.0	0.012	4.1176	52.7	9.34
7	403	60.0	0.016	3.0882	69.6	7.93
8	403	60.0	0.024	2.0418	103.5	5.80
9	413	36.0	0.014	3.4314	69.5	11.78
10	413	45.0	0.018	2.7149	69.5	9.45
11	413	60.0	0.024	2.0588	69.5	6.21
12	413	75.0	0.030	1.6471	69.5	4.16
13	413	60.0	0.012	4.1176	52.7	10.47
14	413	60.0	0.016	3.0882	69.6	9.98
15	413	60.0	0.024	2.0418	103.5	7.68
16	413	60.0	0.048	1.0251	196.1	5.13
17	423	45.0	0.018	2.7149	69.5	11.37
18	423	60.0	0.024	2.0588	69.5	8.36
19	423	75.0	0.030	1.6471	69.5	6.22
20	423	90.0	0.036	1.3725	69.5	4.22
21	423	60.0	0.016	3.0882	69.6	12.55
22	423	60.0	0.024	2.0418	103.5	11.24
23	423	60.0	0.032	1.5345	135.4	9.49
24	423	60.0	0.048	1.0251	196.1	7.49

[a] 3Cu1Ce/AC catalyst (80-100 mesh), 0.1 g; 2 MPa; F_{H2}, flow rate of hydrogen; $F_{crotonaldehyde}$, flow rate of crotonaldehyde; $P_{crotonaldehyde}$, partial pressure of crotonaldehyde; $Y_{condensation}$, overall yield of hydrogenation products including butyraldehyde, crotonyl alcohol and butanol.

23. The rate constants and reaction orders of different temperature for various reactions

Table S7. The rate constants and reaction orders at different temperatures for various reactions[a]

Ethanol dehydrogenation	T (K)	$\ln k_1$ [μmol/ (g·s·kPa^{n1})]	n_1
	483	6.53583	-0.50
	503	6.92242	-0.44
	523	7.15237	-0.46
Acetaldehyde condensation	T (K)	$\ln k_2$ [μmol/ (g·s·kPa^{n2})]	n_2
	483	-4.67110	0.97
	503	-3.93211	1.06
	523	-3.33666	0.97
Crotonaldehyde hydrogenation	T (K)	$\ln k_3$ [μmol/ (g·s·kPa^{n3})]	n_3
	403	-3.26926	1.04
	413	-3.18846	1.00
	423	-3.09440	0.99

[a] k_1, n_1, k_2, n_2, k_3 and n_3, rate constants and reaction orders of ethanol dehydrogenation, acetaldehyde condensation and crotonaldehyde hydrogenation

24. The apparent activation energies and frequency factors for various reactions

Table S8. The apparent activation energies and frequency factors for various reactions

	Ethanol dehydrogenation	Acetaldehyde condensation	Crotonaldehyde hydrogenation
Ea (KJ/mol)	32.5	70.1	12.4
A [μmol/ (g·s·kPa^{ni}), i=1,2 and 3]	228267.3	364707.2	1.3

25. The Guerbet reaction pathway

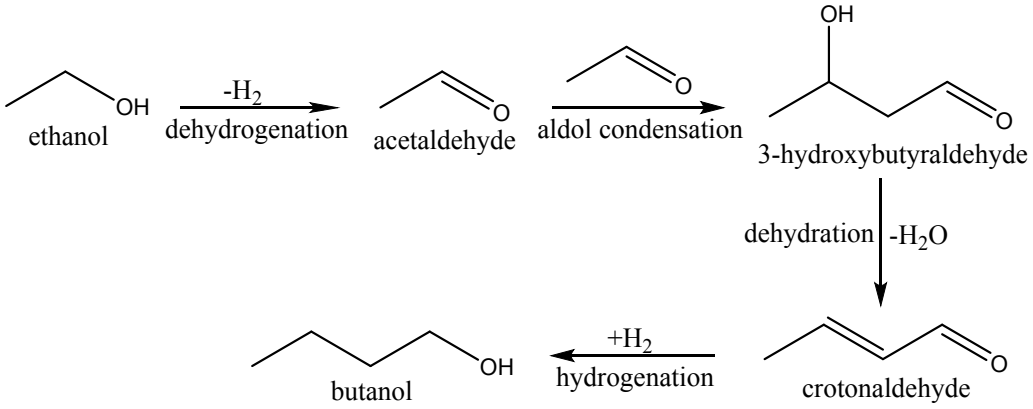

Scheme S1. The Guerbet reaction pathway

26. The hydrogen-transfer pathway

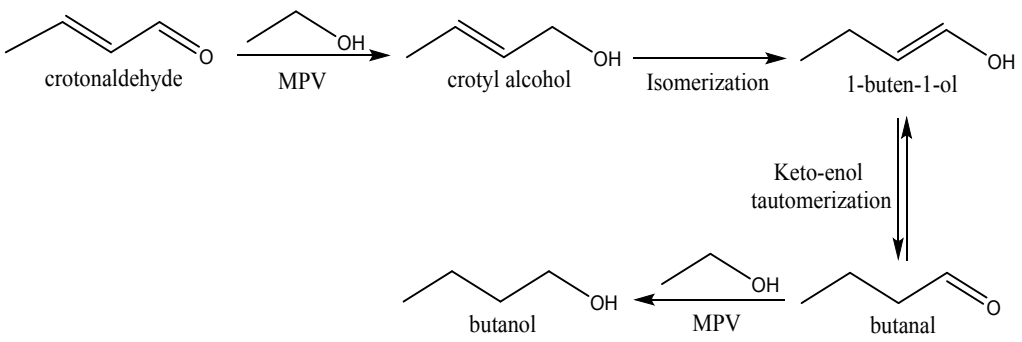

Scheme S2. The hydrogen-transfer pathway

The Meerwein–Pondorf–Verley (MPV) hydrogen-transfer reaction, which is catalyzed by Lewis acids or bases, is an important reaction for the hydrogenation of crotonaldehyde to butanol. According to the study by Bell et al. [ACS Catal. 2016, 6, 939-948], the hydrogen-transfer pathway between crotonaldehyde and ethanol is shown in Scheme S2.

It seems that the hydrogenation of crotonaldehyde prefers C=O reduction to form crotyl alcohol in the MPV reaction, probably due to the involvement of surface hydrides [C. Copéret et al. Chem. Rev. 2016, 116, 8463-8505]. Thus, the presence of crotyl alcohol is likely the indictor of occurrence of MPV-type reactions. However, no crotyl alcohol was detected in our work. Moreover, the formation of H atoms instead of hydride species is more favorable on reducible materials such as CeO_2 and TiO_2, due to their small band gap easing the formation of hydroxyls and transfer of electrons to the conduction band when contacting with H_2 [C. Copéret et al. Chem. Rev. 2016, 116, 8463-8505]. Therefore, the introduction of CeO_2 did not facilitate the MPV reaction in our reaction system. CeO_2 mainly contributed to the enhanced condensation activity as basic sites. This statement can be verified by the product distribution of CeO_2/AC catalyst as shown in Table S2, where no crotyl alcohol while high selectivity towards crotonaldehyde is observed.

To compare the rates of C=C vs C=O hydrogenation, we investigated the dependence of hydrogenation of pure crotonaldehyde on reaction temperature in the presence of H_2 over 3Cu1Ce/AC catalyst. The result presented in Figure S8 illustrates the major intermediate of the hydrogenation of crotonaldehyde is butyraldehyde, as a result of C=C hydrogenation over the reaction temperatures of 393-473K. Thus, the hydrogenation rate of C=C is much fast than that of C=O. Increasing reaction temperature can accelerate the hydrogenation rates of both C=C and C=O. Although higher reaction temperature (>473 K) was also applied in this investigation, a severe catalyst deactivation due to the polymerization of crotonaldehyde was observed, which may alter the composition of active sites of 3Cu1Ce/AC catalyst, thus the result is not

presented here. On the contrary, in the ethanol upgrading reaction, once crotonaldehyde was formed, it could be rapidly hydrogenated. Therefore, no crotonaldehyde was detected and the Cu-Ce/AC catalysts were stable over 12 h.

Based on the above discussion, we propose H atoms from the dehydrogenation of ethanol are the main H source for the hydrogenation reaction, especially in the absence of any external H_2 gas in the reactant stream. Although both Cu metals and CeO_2 in Cu-Ce/AC are able to dehydrogenate ethanol to form H atoms, Cu metals have much higher reactivity than CeO_2. In this context, once crotonaldehyde is formed on CeO_2, it migrates to Cu metals where the hydrogenation of C=C bonds of crotonaldehyde takes place and generates butyraldehyde as the major intermediate.